SUPPORTING INFORMATION

Non-Invasive Optical Guided Tumor Metastasis/Vessel Imaging by Using Lanthanide Nanoprobe with Enhanced Down-Shifting Emission Beyond 1500 nm

Youbin Li[†], *Songjun Zeng*[†]*, *Jianhua Hao*[‡]*

[†]*Synergetic Innovation Center for Quantum Effects and Application, Key Laboratory of Low-dimensional Quantum Structures and Quantum Control of Ministry of Education, School of Physics and Electronics, Hunan Normal University, Changsha, 410081, P.R. China.*

[‡] *Department of Applied Physics, The Hong Kong Polytechnic University, Hong Kong (China)*

Corresponding Author:

songjunz@hunnu.edu.cn, jh.hao@polyu.edu.hk

Characterizations. The crystal phase of the as-prepared samples were characterized by using XRD (Rigaku D/max 2500 X-ray diffractometer) with Cu-Kα radiation (λ = 0.15406 nm) at 40 kV and 250 mA. The shape and structure were characterized by a TEM (FEI Tecnai F20) at an acceleration voltage of 200 kV. UC luminescence spectra were measured by a Zolix spectrophotometer (fluoroSENS 9000A) system upon the excitation of 980 nm laser. The downshifting NIR-IIb spectra of the samples were measured with a NIR-II spectroscopy (NIRQuest512, Ocean Optics) upon the excitation of 980 nm laser at room temperature. The XPS spectra were collected by using a Escalab 250Xi spectrometer with a mono X-Ray source Al Kα excitation. The DLS and zeta potential of the as-prepared samples were recorded on a Zetasizer Nano ZS at room temperature.

Animal Models. 8×10^6 LLC cells were first subcutaneously injected into a BALB/C mouse for further culture to obtain the tumor-bearing mouse model with an average tumor size of 4 mm for small tumor diagnosis. 8×10^6 LLC cells were subcutaneously injected into BALB/C nude mice for further culture to obtain the tumor model with an average tumor size of 1.2 cm in original injected tumor site for optical imaging-guided tumor vascular/metastasis and high-magnification tumor vascular imaging, respectively. 8×10^6 HCT116 cells were also subcutaneously injected into BALB/C nude mice for further culture to obtain another tumor model for tumor vessel imaging.

***In Vitro* X-Ray Phantom and *In Vivo* CT Bioimaging:** To evaluate the X-ray contrast efficiency, PAA-Lu-NRs and Iobitridol were dispersed in water with different Lu and I concentrations ranging from 0 to 30 mg/mL, respectively. *In vitro* phantom X-ray imaging was demonstrated by using a multimodal imaging system (Bruker *In Vivo* FX pro) with parameters:

voltage-45 kVp; aluminium filter-4 mm, and exposure time-30 s. *In vivo* CT bioimaging of Kunming mouse was further performed by using a small animal CT imaging system (Quantum GX2 micro-CT imaging system, PerkinElmer). After intravenous injection of PAA-Lu-NRs solution (200 μL, 20 mg/mL), CT images were recorded at different time points (10 min, 2 h, 12 h, 24 h). The imaging parameters were as following: tube voltage-90 kV, tube current-80μA, field of view-72 mm, and pixel size-144 μm.

NIR-IIb Optical Bioimaging of Small Tumor Detection. The NIR-IIb bioimaging was demonstrated by using a small animal imaging system[s1,s2] (*In Vivo* Master, Wuhan Grand-imaging Technology Co., LTD) equipped with a thermoelectric cooled InGaAs camera (Model: NIRvana™ Camera System, operating temperature: -80 ℃, Princeton Instruments). Excitation light was provided by a 980 nm diode laser and filtered by a (1400-1600 nm) band pass filter. 150 μL of pentobarbital sodium aqueous solution (10 wt%) was intraperitoneally injected into the tumor-bearing mouse to anesthetize it. 200 μL of PAA-modifying $NaLuF_4$ solution with a concentration of 3 mg/mL was intravenously injected into the tumor-bearing mouse (tumor size: ~ 4 mm) for tumor detection. The NIR-IIb fluorescence imaging was performed with the *in vivo* imaging system as mentioned. The excitation intensity of the 980 nm laser was about 100 mW/cm^2. *Ex-vivo* bioimaging of the tumor and isolated organs were executed by the same parameters. The digital picture of the tumor was taken by using a Canon digital camera. All animal procedures obeyed the Guidelines for the Care and Use of Laboratory Animals of Hunan Normal University and approved by the Animal Ethics Committee of Hunan Province.

NIR-IIb Blood Vessel Imaging. NIR-IIb dynamic brain vessel imaging, whole-body blood vessel imaging of the Kunming mouse and tumor vessel imaging of the nude mouse (tumor size: 1.2 cm) were performed by using the same NIR-IIb bioimaging system (NIR-II lens: 100 mm,

Edmund Optics, FOV: 26 mm×21 mm, 640×512 pixels, 41 μm/pixel). 200 μL (3 mg/mL) PAA-Lu-NRs solution was first intravenously injected into an anesthetized Kunming mouse for fluorescent-based vascular imaging. Then we collected the vascular fluorescence signal by using the same imaging system equipped with a fiber-coupled 980 nm laser as light resource. The average intensity of the 980 nm laser was about 100 mW/cm^2.

Pharmacokinetics and Biodistribution Test of PAA-Lu-NRs. Kunming mice were used for evaluating the pharmacokinetics and bio-distribution of PAA-Lu-NRs (n= 3 mice/group). For *in vivo* bioimaging, the PAA-Lu-NRs (200 μL, 3 mg/mL) were first injected into the Kunming mice through tail vein. The fluorescence signals were recorded by using the same system under 980 nm excitation with an excitation power density of 100 mW/ cm^2. And the corresponding organs of the mice (heart, Liver, spleen, lung, kidney) were collected after 2, 6, 12, 24, and 48 h injection for *ex-vivo* NIR-IIb bioimaging by using the same system.

The blood half-life time was performed based on the blood fluorescence intensity according to previous report[s3]. The Kunming mice were first intravenously injected with PAA-Lu-NRs (200 μL, 3 mg/mL), the blood samples were collected at time points from 1 min to 24 h with same volume of 50 μL. The content of the PAA-Lu-NRs in blood was evaluated by recording the fluorescence intensity under the excitation of 980 nm laser with power density of 100 mW/ cm^2.

Quantum Yield Measurement. The fluorescence QY of the 5 % Ce doped $NaLnF_4$ nanorods in cyclohexane and water were calculated in a similar way to the reported papers using a standard IR-26 dye (dissolved in DCE, QY = 0.5%) as a reference:[s4]

$$\Phi_s = \Phi_r (F_s/F_r) *(A_r/A_s)*(n^2_s/n^2_r),$$

where Φ represents quantum yield, F denotes integrated photoluminescence emission intensity, A denotes absorbance at the maximum excitation wavelength and n is the refractive index of the

solvent (n= 1.42 for cyclohexane, n = 1.44 for DCE, n= 1.33 for water, respectively). The subscripts s and r represents the sample and reference solutions, respectively.

Histology Analysis. For histology analysis, Kunming mice intravenously injected with 200 μL (3 mg/mL) of PAA-Lu-NRs solution after 3 days, 7 days, 30 days and control group were dissected. The obtained isolated organs including heart, liver, spleen, lung, and kidney were stained with hematoxylin and eosin (H&E) for further characterization. The colorectal and LLC tumor-bearing nude mice after 48 h intravenous injection of PAA-Lu-NRs were sacrificed, and the tumor sections were stained with H&E for histology analysis. The bio-TEM micrographs of the LLC tumor sections were also detected by a TEM (FEI Tecnai F20).

Immune Response Test. Healthy Kunming mice were divided into two groups (n=10 per group) at random. The control group mice were intravenously injected with 200 μL of PBS. The test group mice were injected with PAA-Lu-NRs (200 μL, 3 mg/mL) through the tail vein. The weights of the mice were further recorded after 48 h injection and then sacrificed to collect the main organs (Liver, Spleen, and Thymus). The Liver, spleen and thymus indexes of the control and test group mice were measured by the following formula:[s5]

$$\text{Organ index (mg/g)} = \text{organ weight (mg)}/\text{mouse weight (g)}$$

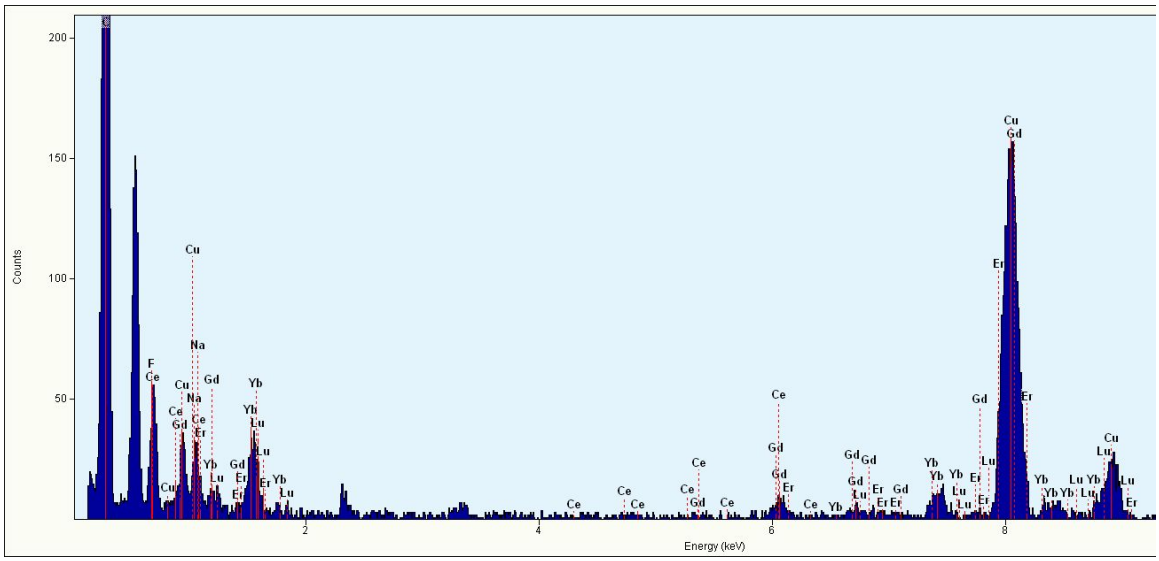

Figure S1. EDS pattern of the as-prepared $NaLuF_4$:20Yb/2Er/40Gd/5%Ce nanorods.

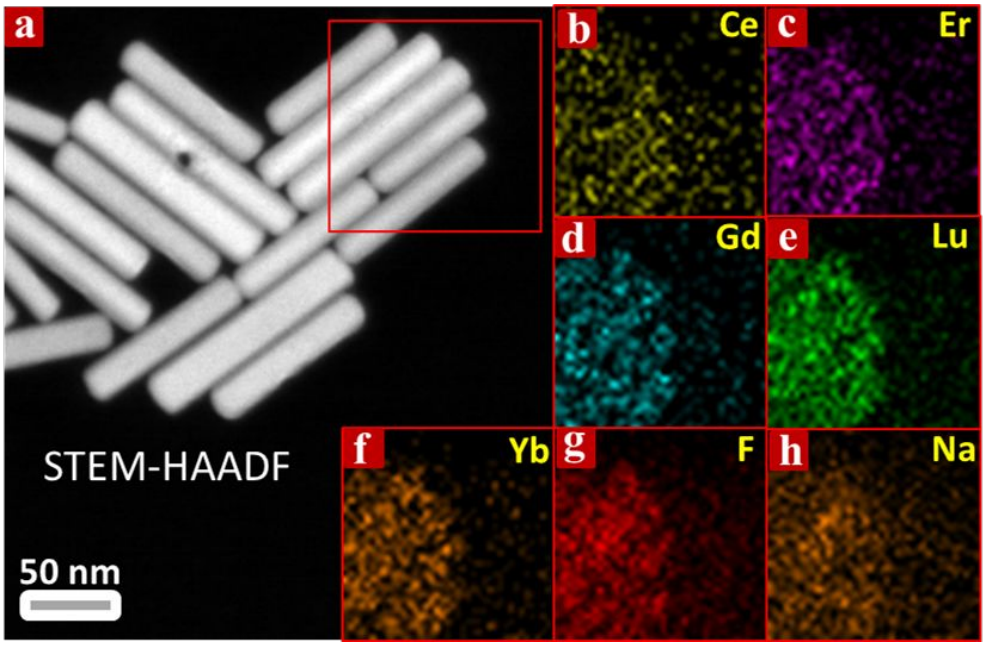

Figure S2. (a) The typical STEM image of the as-prepared $NaLuF_4$:20Yb/2Er/40Gd/5Ce nanorods. The EDS mapping results of different elements in (a) were marked by red rectangle: (b) Ce, (c) Er, (d) Gd, (e) Lu, (f) Yb, (g) F, (h) Na.

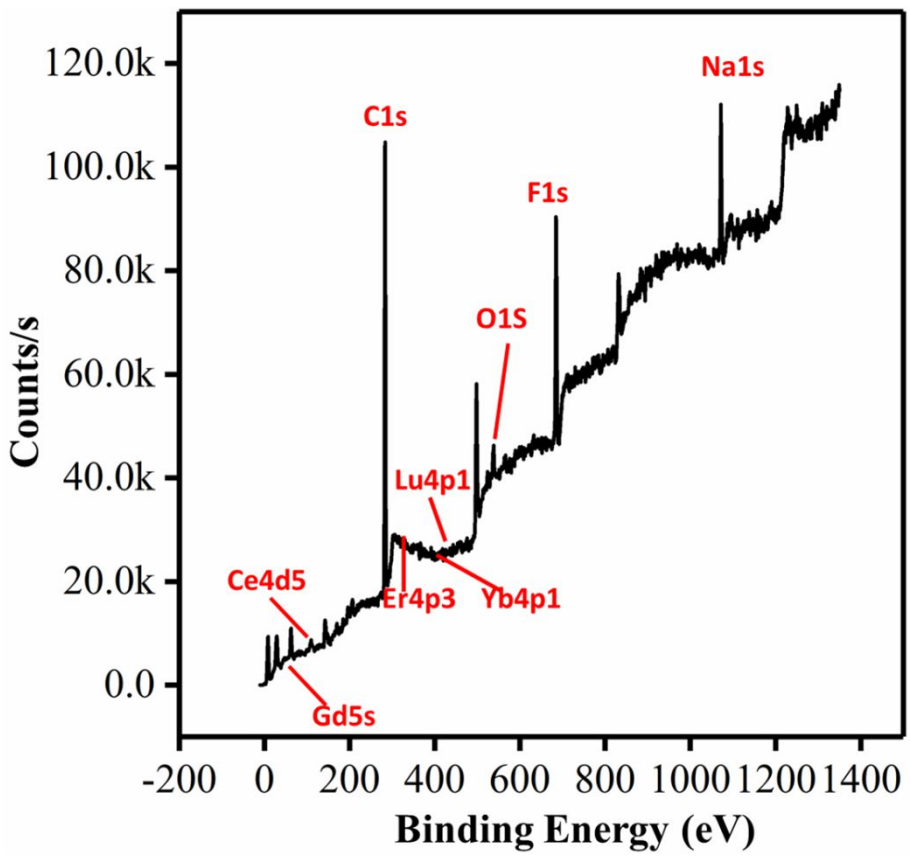

Figure S3. The XPS spectrum of the as-synthesized $NaLuF_4$:40Gd/20Yb/2Er/5%Ce. The 5s level of Gd at 38 eV, the 4d level of Ce at 110 eV, the 1s level of C at 286.6 eV, the 4p level of Er at 315 eV, the 4p level of Yb at 391 eV, the 4p level of Lu at 418 eV, the 1s level of O at 532 eV, the 1s level of F at 684 eV, the 1s level of Na at 1072 eV.

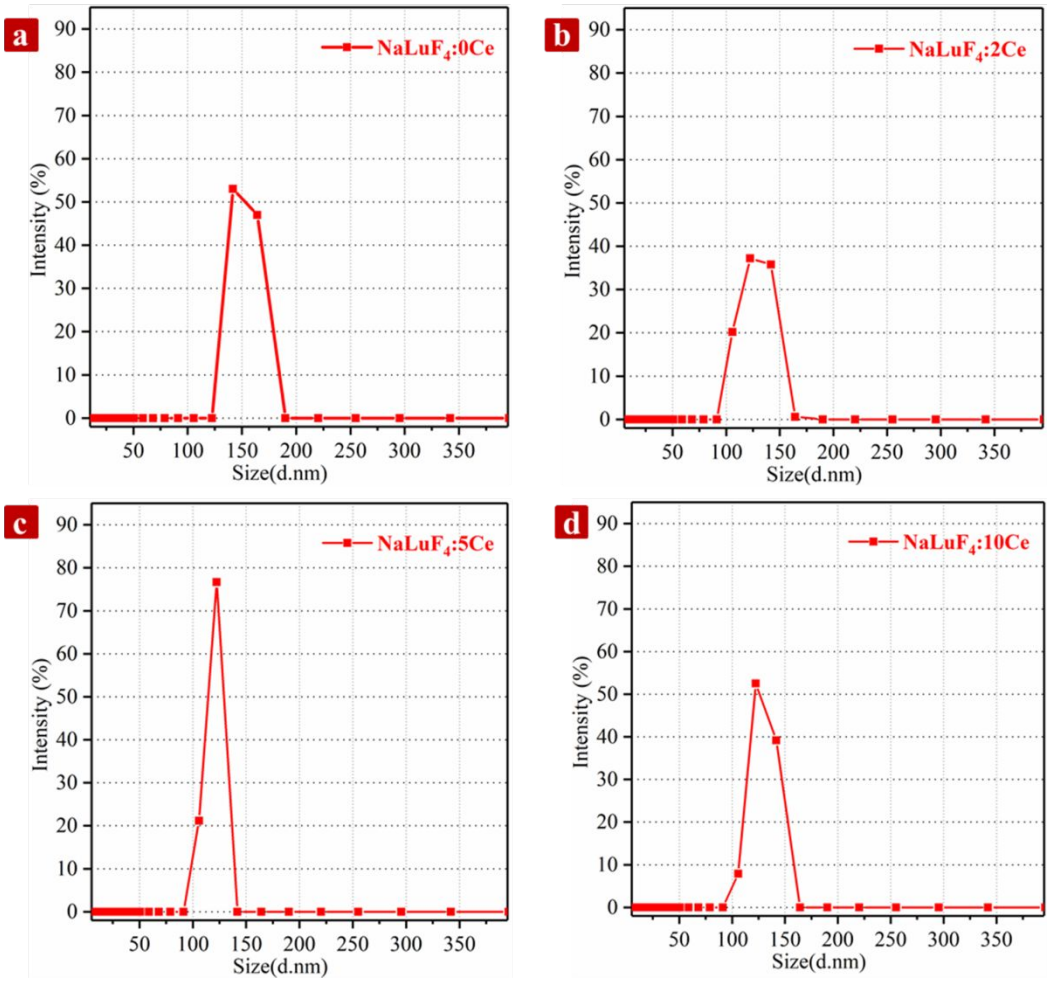

Figure S4. DLS measurements of the $NaLuF_4$:40Gd/20Yb/2Er nanorods doped with different Ce^{3+}: (a) 0%, (b) 2%, (c) 5%, (d) 10%.

Table S1. The lattice constants of the $NaLuF_4$:40Gd/20Yb/2Er/xCe nanorods (x= 0, 2, 5, 10%).

$NaLuF_4$:20Yb/2Er/40Gd/XCe	a/b(Å)	c(Å)
0	6.00401	3.54062
2	6.02412	3.54469
5	6.02544	3.55075
10	6.02642	3.56976

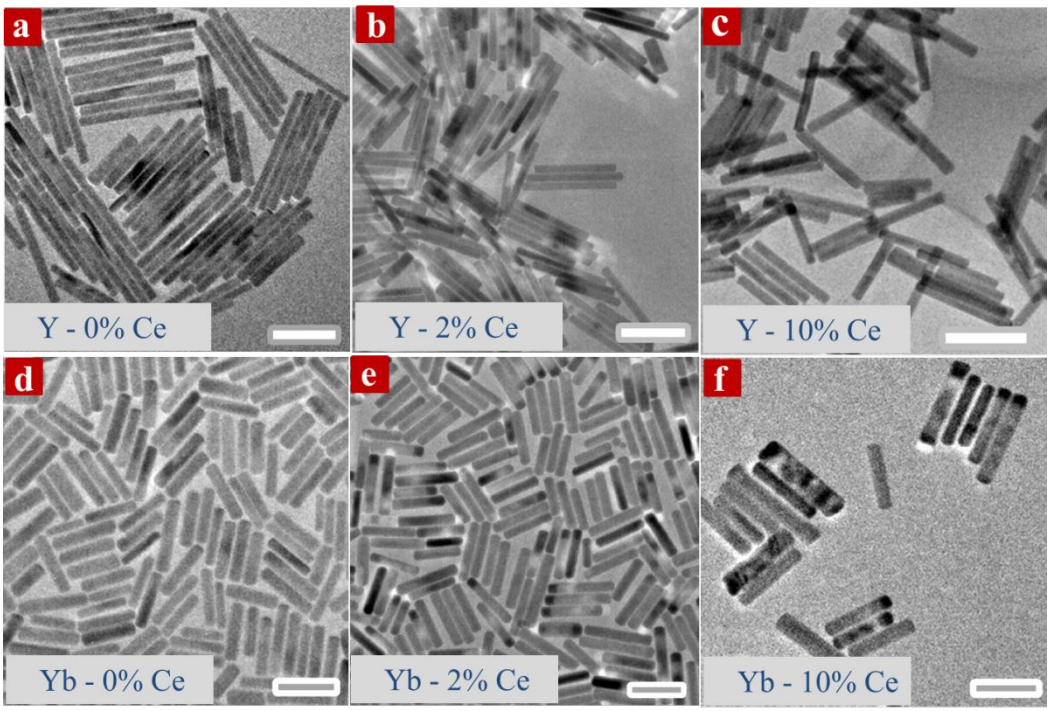

Figure S5. (a), (b) and (c) TEM images of the $NaYF_4$:20Yb/40Gd/2Er samples doped with different concentrations of Ce^{3+} (0, 2, 10 mol%), respectively. (d), (e) and (f) TEM images of the as prepared $NaYbF_4$:40Gd/2Er samples doped with different contents of Ce^{3+} (0, 2, 10 mol%), respectively.

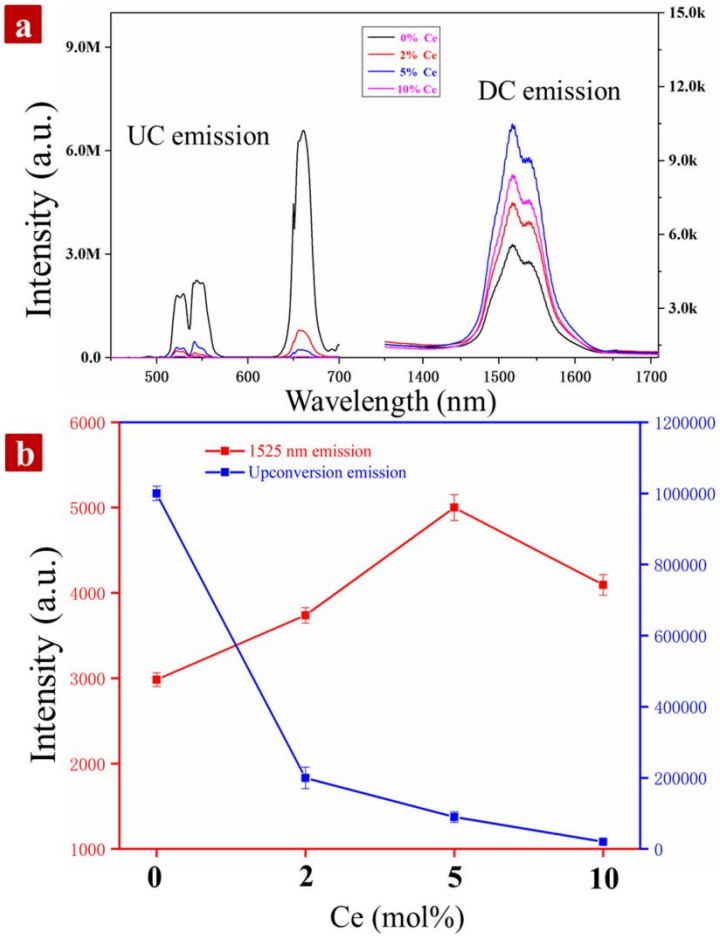

Figure S6. (a) UC and NIR-IIb luminescence spectra of $NaYF_4$:40Gd/20Yb/2Er samples doped with different contents of Ce^{3+} (0, 2, 5, 10 mol%). (b) The integrated intensity for NIR-IIb emission bands at 1525 nm and UC emission bands at 535 nm and 650 nm.

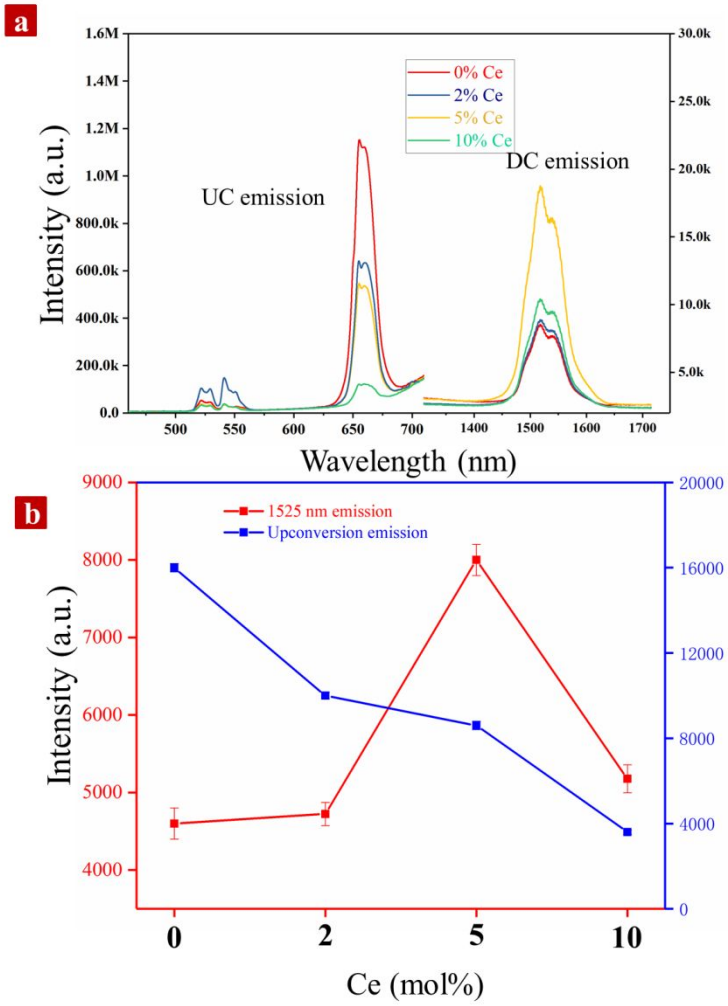

Figure S7. (a) UC and downshifting luminescence spectra of $NaYbF_4$:40Gd/2Er samples doped with different contents of Ce^{3+} (0, 2, 5, 10 mol%). (b) The integrated intensity for downshifting emission bands at 1525 nm and UC emission bands at 535 nm and 650 nm.

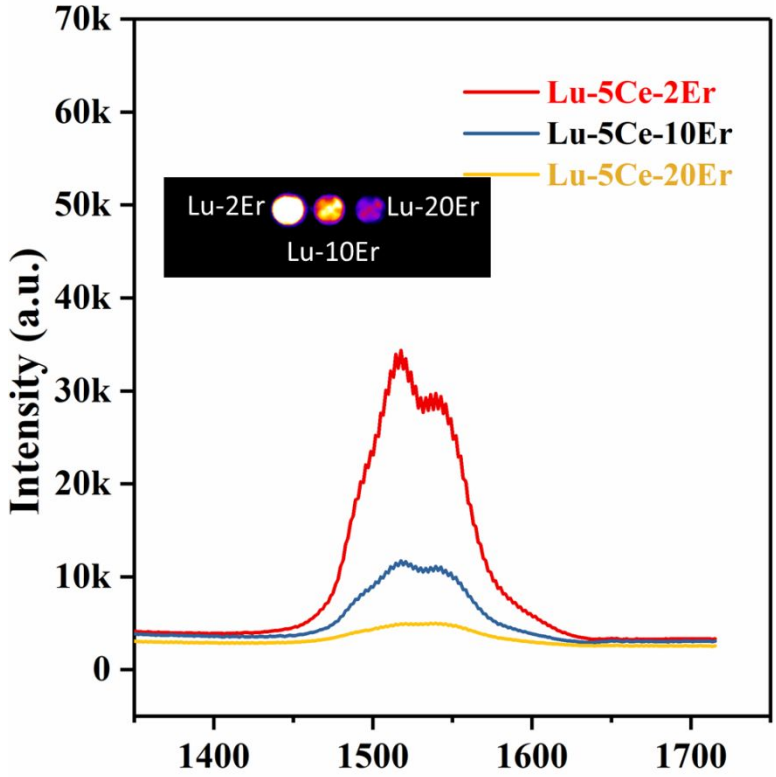

Figure S8. Downshifting emission of the as-prepared $NaLuF_4$:40Gd/20Yb/2Er/5%Ce nanorods doped with different concentrations of Er^{3+}. The inset presents the corresponding *in vitro* phantom imaging.

Table S2. The quantum efficiency (QY) of the 5% Ce doped $NaLnF_4$ nanocrystals in cyclohexane and water.

Host \ QY	cyclohexane	water
$NaLuF_4$:5%Ce	26%	3.6%
$NaYbF_4$:5%Ce	22.4%	3.0%
$NaYF_4$:5%Ce	16%	2.2%

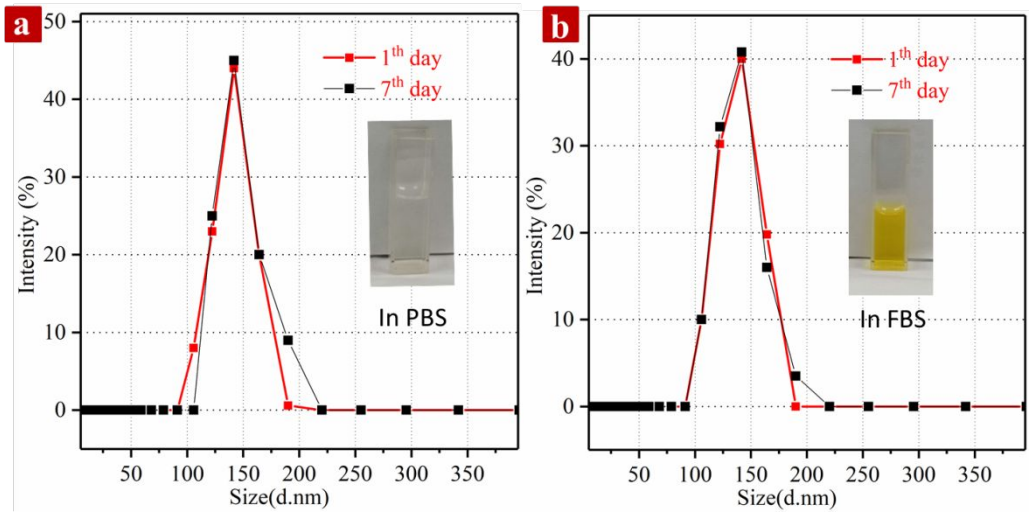

Figure S9. Stability of PAA-Lu-NRs dispersed in (a) PBS and (b) FBS solution. The insets in (a) and (b) indicate the corresponding digital photograph of PBS and FBS solution containing PAA-Lu-NRs, respectively.

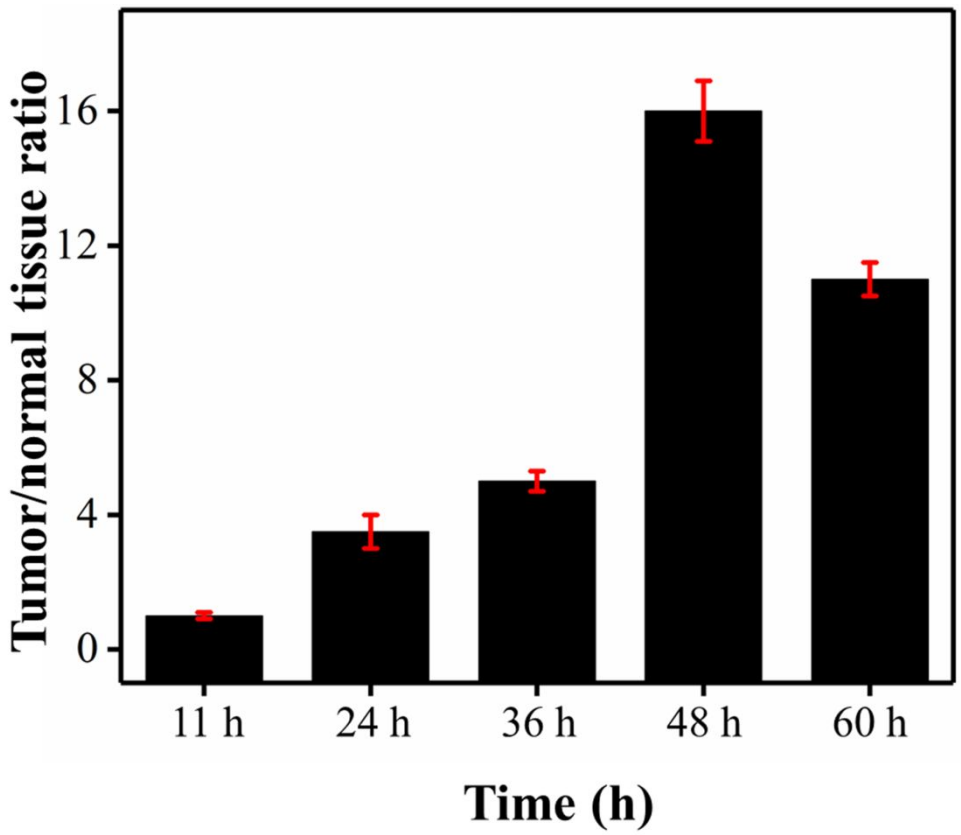

Figure S10. The tumor to normal tissue ratio of the LLC tumor-bearing mice at different time points.

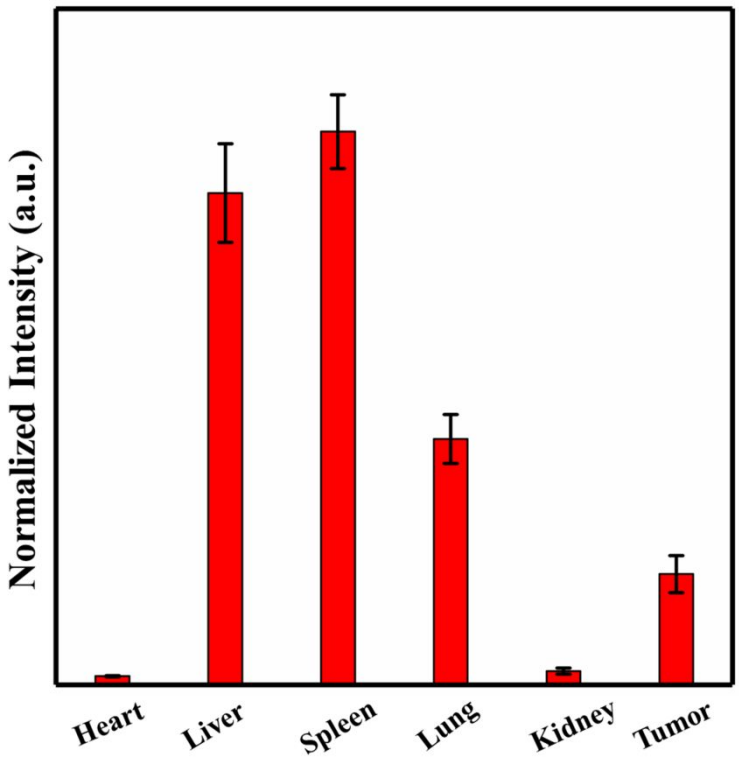

Figure S11. Biodistribution of PAA-Lu-NRs in the LLC tumor-bearing BALB/C mice after 48 h injection. The data were analyzed based on the fluorescence intensity.

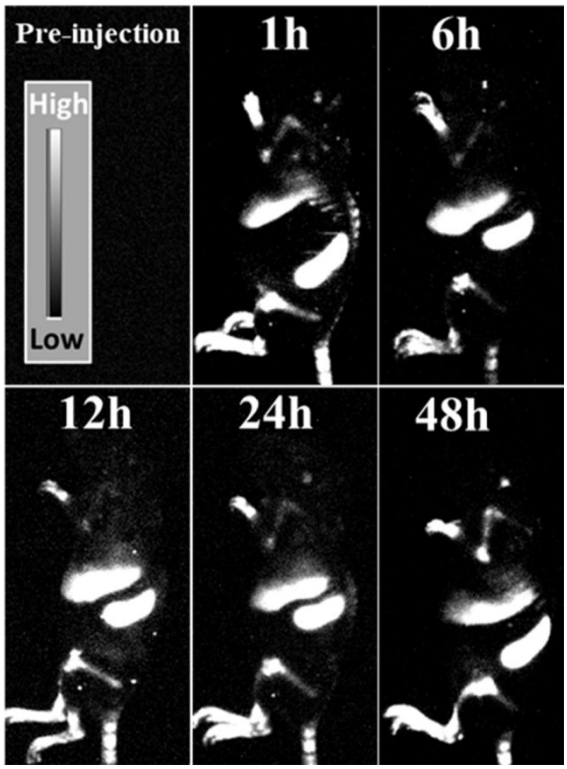

Figure S12. Time-dependent NIR-IIb bioimaging of Kunming mouse after intravenous injection of PAA-Lu-NRs under 980 nm laser excitation with power density of 100 mW/cm^2.

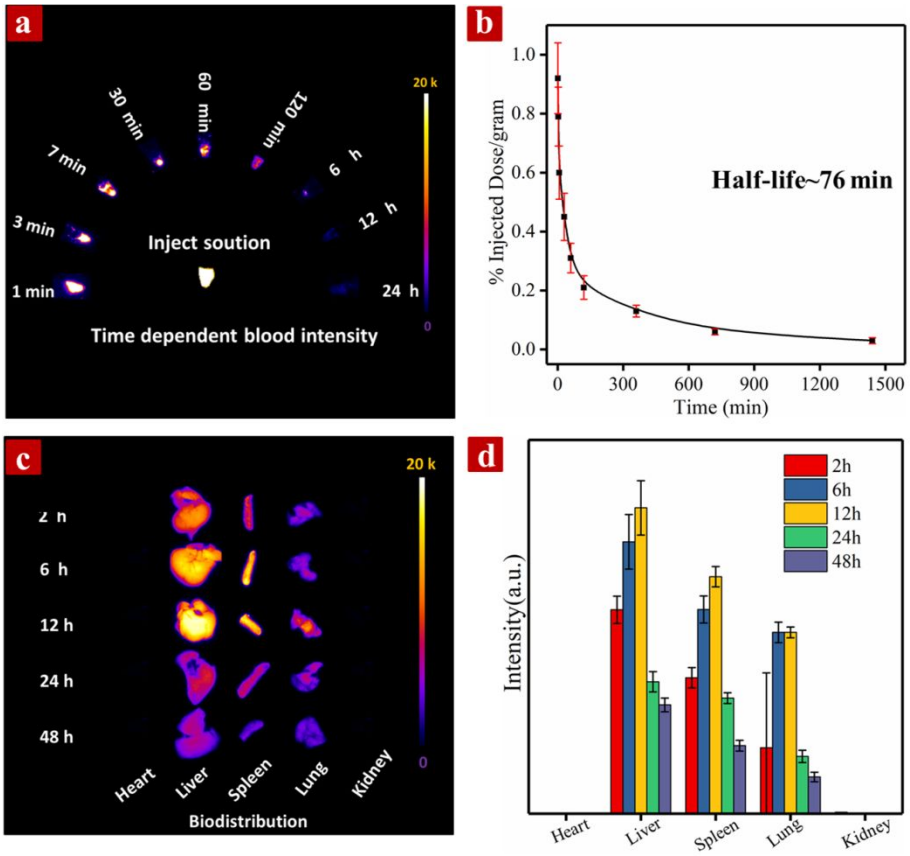

Figure S13 (a) Time-dependent blood fluorescence signal after intravenous injection of the P AA-Lu-NRs in 24 h under 980 nm laser excitation with power density of 100 mW/cm^2. (b) Time course of PAA-Lu-NRs contents in blood (based on the fluorescence intensity). (c) *Ex-vivo* NIR-IIb fluorescent imaging of main organs from the mice treated with PAA-Lu-NRs after 2 h, 6 h, 12 h, 24 h and 48 h post-injection under 980 nm laser excitation with power density of 100 mW/cm^2. (d) Biodistribution of PAA-Lu-NRs in the main organs from the treated mice after 2 h, 6 h, 12 h, 24 h and 48 h post-injection.

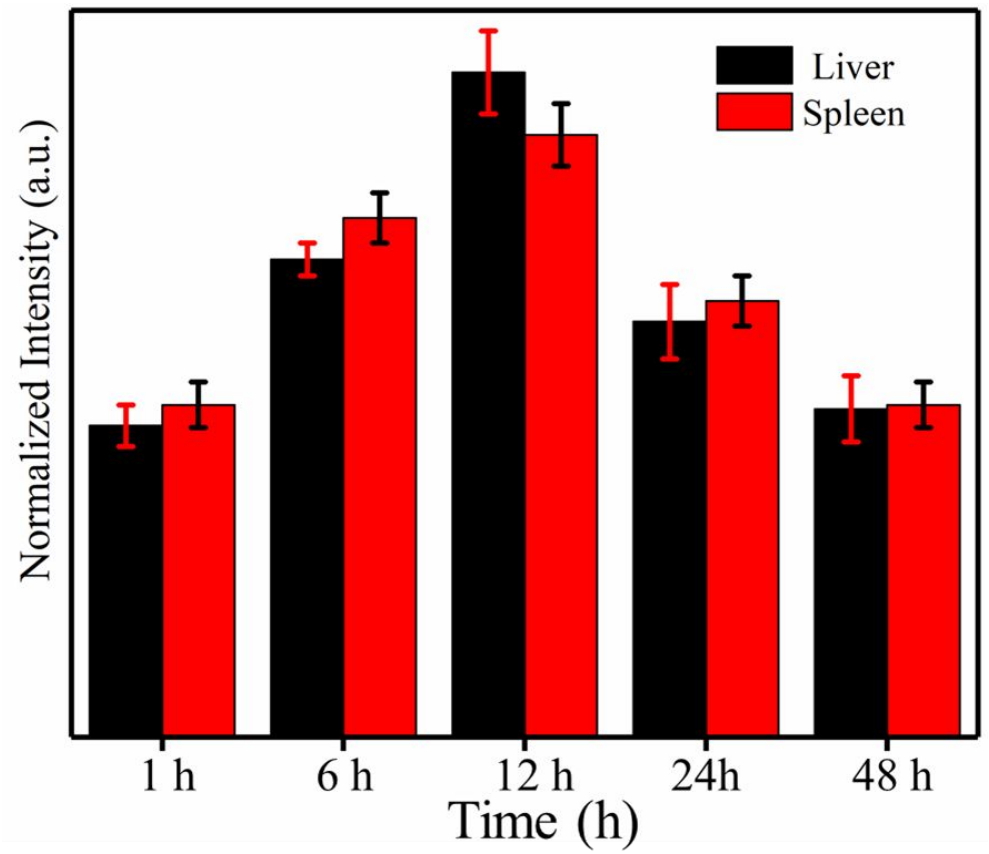

Figure S14. Time-dependent fluorescence intensity of Kunming mouse organs (liver and spleen) taken from Figure S12.

Table S3. Effect of contrast agent on immune function of normal animals

Organ index(mg/g)	Control group	Test group
Liver index	**0.5602±0.0337**	**0.6219±0.0613***
Thymus index	**0.3556±0.0708**	**0.2744±0.0636***
Spleen index	**0.0449±0.0112**	**0.0515±0.0149***

Note: *P > 0.05, indicating the negligible immune response compared with the control group

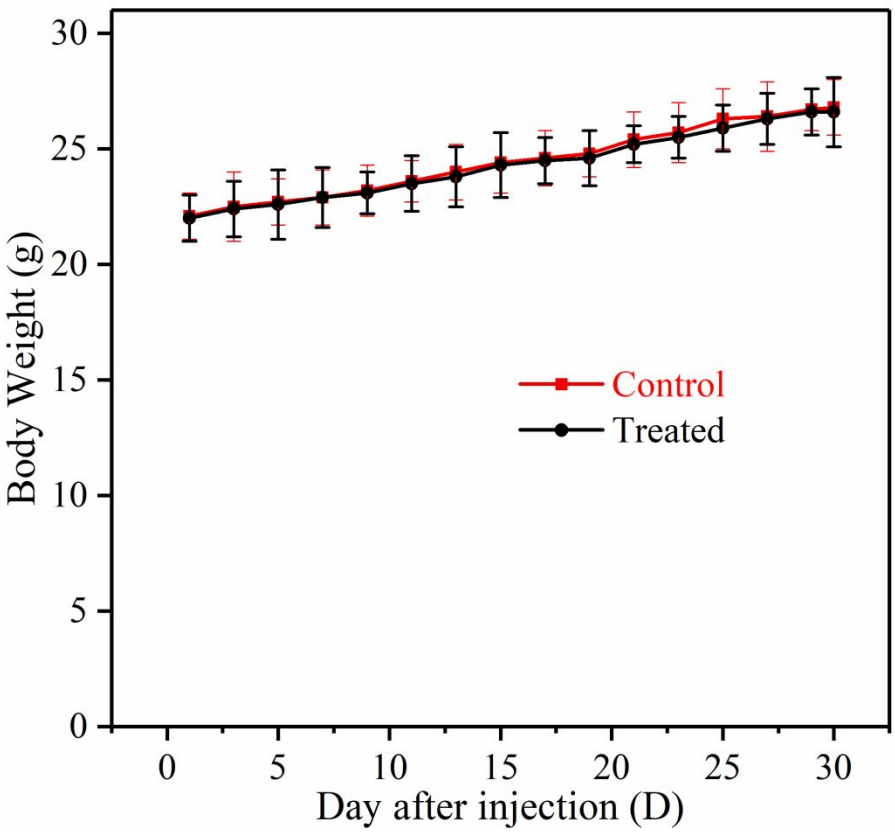

Figure S15. Body weight of the control and PAA-Lu-NRs treated mice (n = 5 mice/group) over a period time of 30 days.

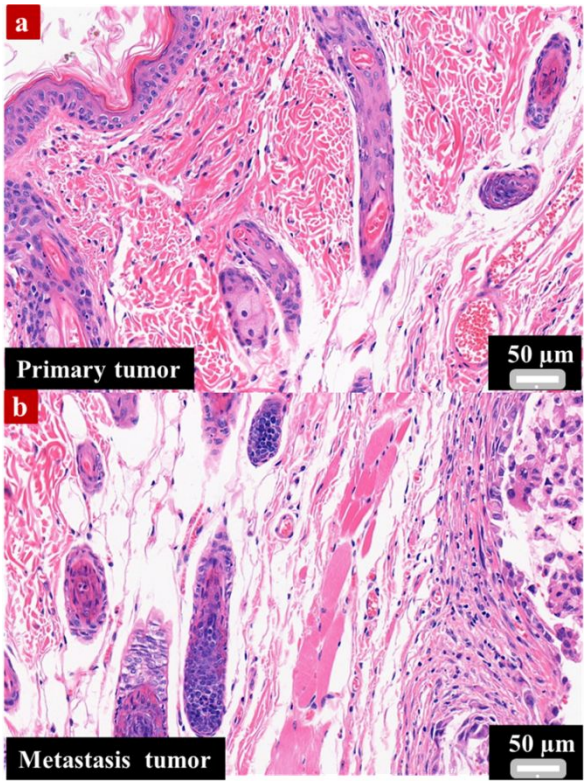

Figure S16. Histological images of H&E stained tumor section: (a) Primary tumor and (b) metastasis tumor dissected from the LLC tumor-bearing mice.

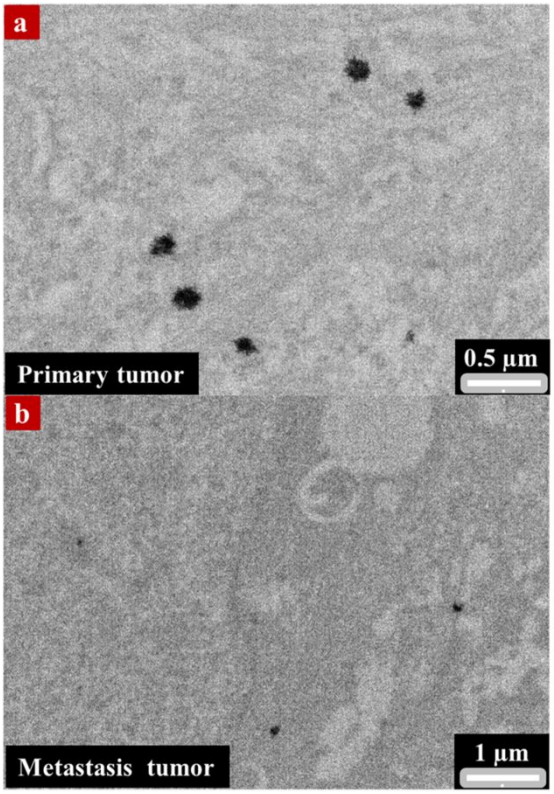

Figure S17. TEM micrographs of tumor sections: (a) Primary tumor, (b) metastatic tumor dissected from the LLC tumor-bearing mice.

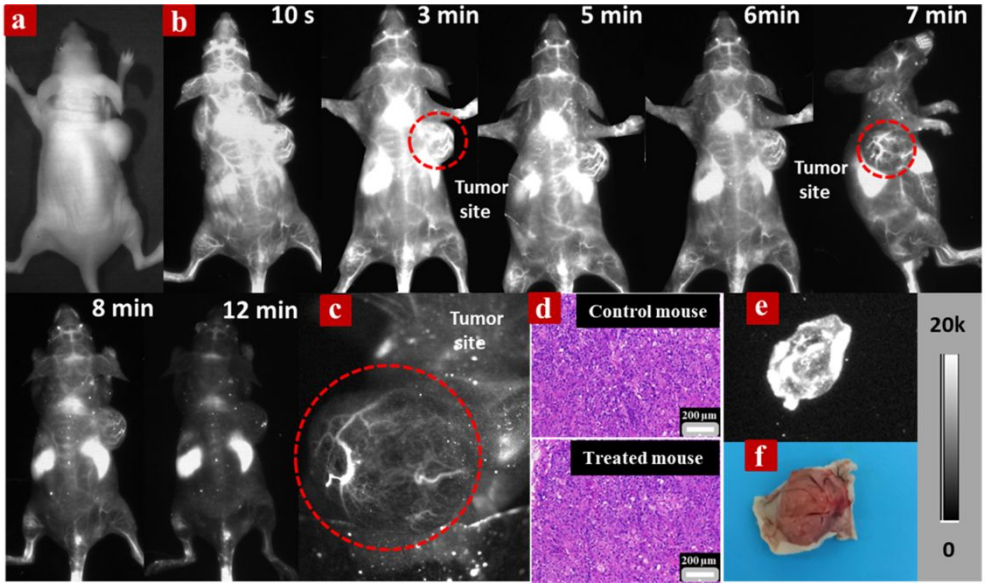

Figure S18. (a) A bright field image of the colorectal tumor-bearing nude mouse. (b) Time coursed NIR-IIb vessel imaging of the colorectal tumor-bearing mouse under 980 nm laser excitation with power density of 100 mW/cm^2. (c) A magnified tumor vessel image (FOV: 26 mm×21 mm). (d) Histological images of the tumor resected from the tumor-bearing mice after 48 h intravenous injection of PAA-Lu-NRs (200 μL, 3 mg/mL) and control group without injection. (e) *Ex vivo* NIR-IIb bioimaging of the resected tumor. (f) A digital photograph of the tumor.

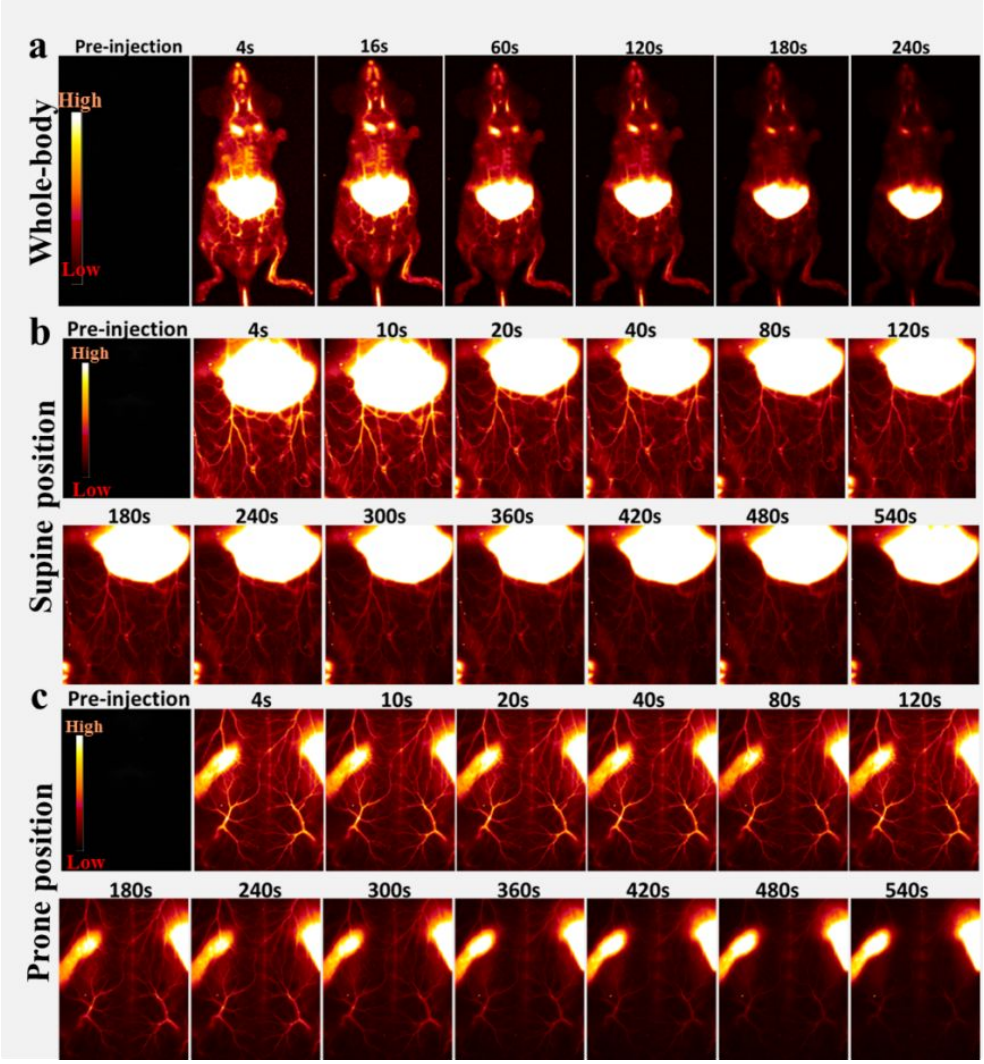

Figure S19. *In vivo* NIR-IIb whole-body vessel imaging of a mouse after intravenous injection with PAA-Lu-NRs. (a), (b) and (c) The whole body (NIR-II lens, field of view (FOV): 14.6 cm×18.3 cm), supine position and prone position (NIR-II lens, FOV: 26 mm×21 mm) vessel image, respectively.

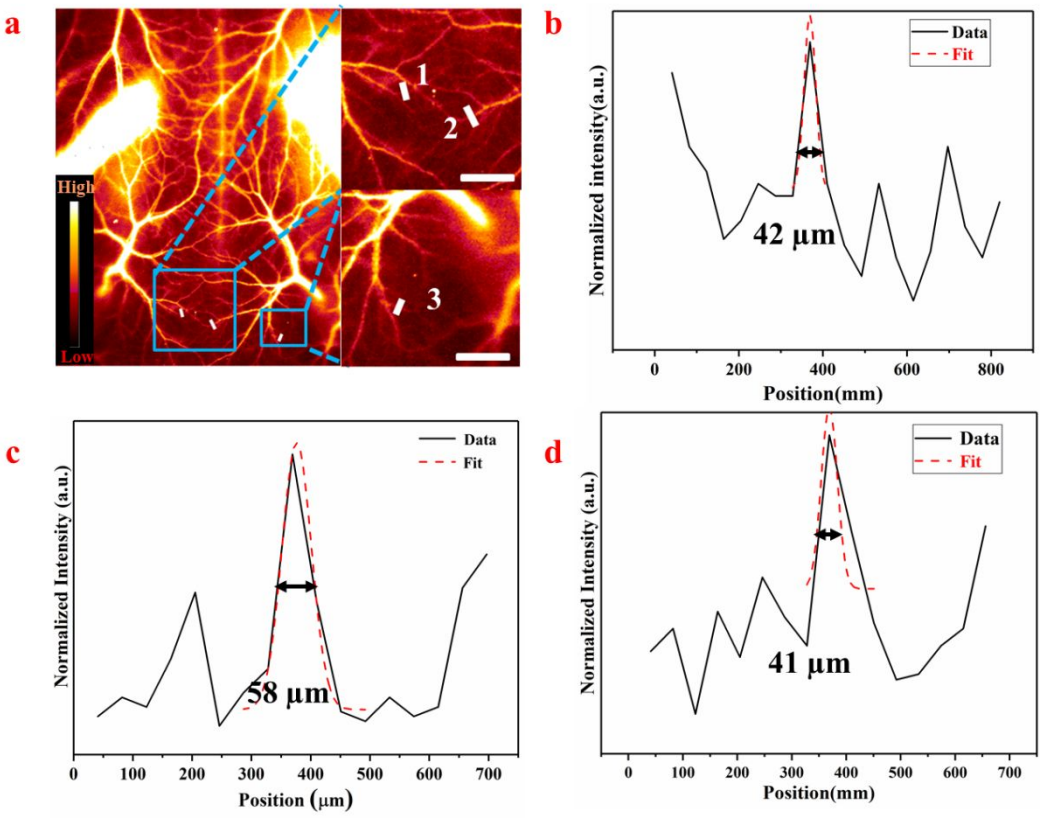

Figure S20 (a) High-magnification NIR-IIb vessel image of a mouse in prone position under a 980 nm laser excitation (NIR-II lens: 100 mm, Edmund Optics, FOV: 26 mm×21 mm, 640×512 pixels, 41 μm/pixel). (b), (c) and (d) The corresponding cross-sectional intensity profiles (black curves), and Gaussian fitting lines (red dashed curves), and full width at half maximum (FWHM) width analysis measured from the white lines marked by 1, 2 and 3 in (a), respectively. All scale bars are 2 mm.

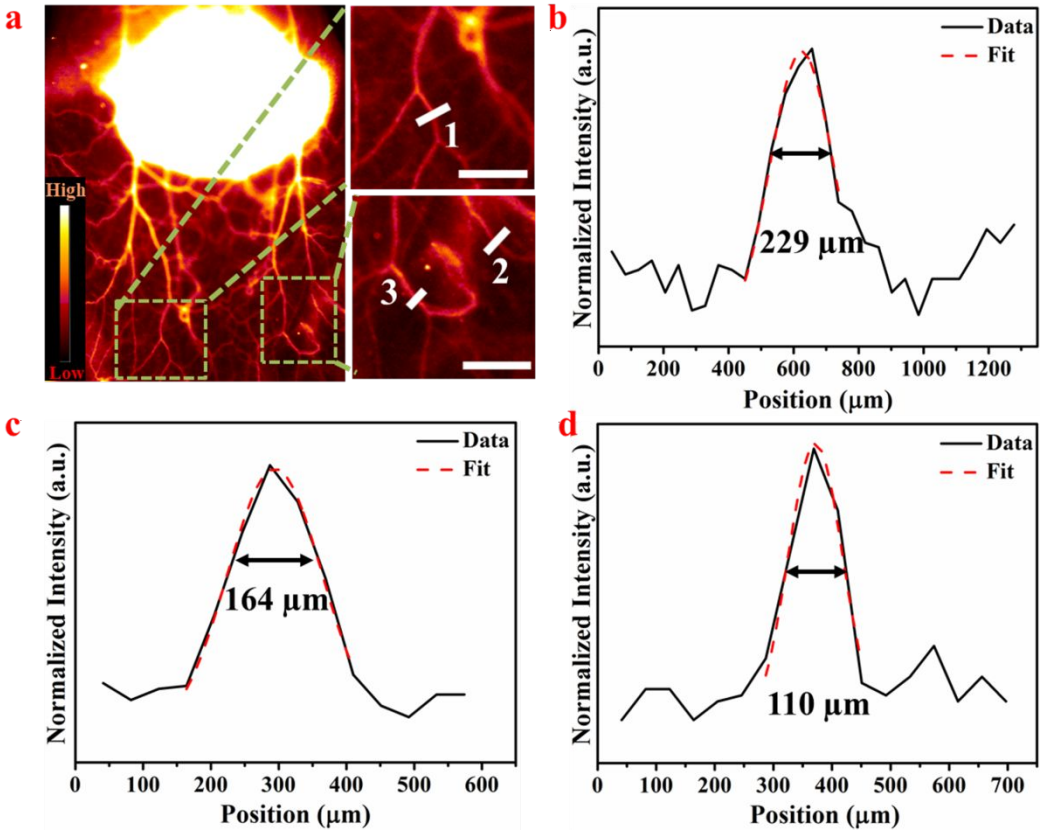

Figure S21. (a) High-magnification NIR-IIb vascular image of supine position under a 980 nm laser excitation (NIR-II lens: 100 mm, Edmund Optics, FOV: 26 mm×21 mm, 640×512 pixels, 41 μm/pixel). (b), (c) and (d) The corresponding cross-sectional intensity profiles (black curves), and Gaussian functional fitting lines (red dashed curves), and FWHM width analysis measured from the white lines marked by 1, 2 and 3 in (a), respectively. All scale bars are 2 mm.

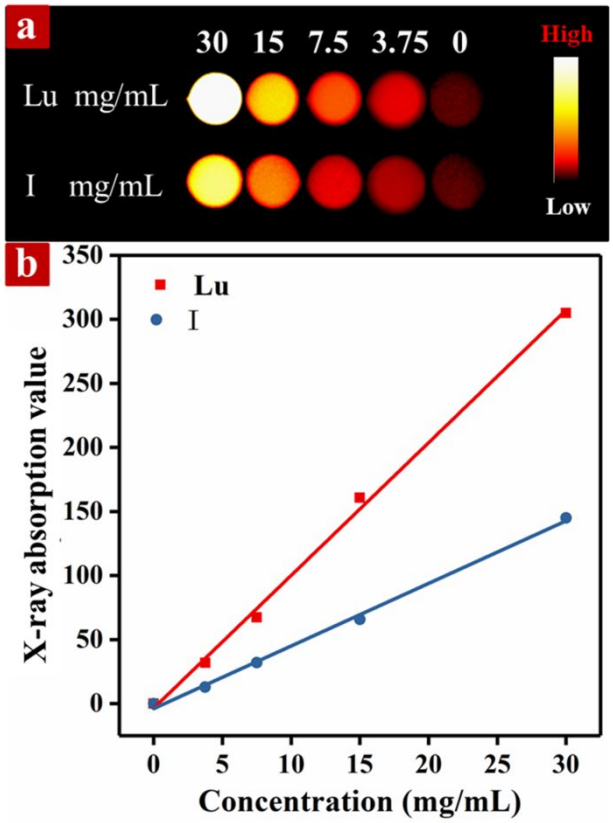

Figure S22. (a) *In vitro* phantom X-ray imaging of PAA-Lu-NRs and iobitridol solution with different contents of Lu and I. (b) Concentration dependent X-ray absorption value of the PAA-Lu-NRs (Lu element, red line) and iobitridol (I element, blue line).

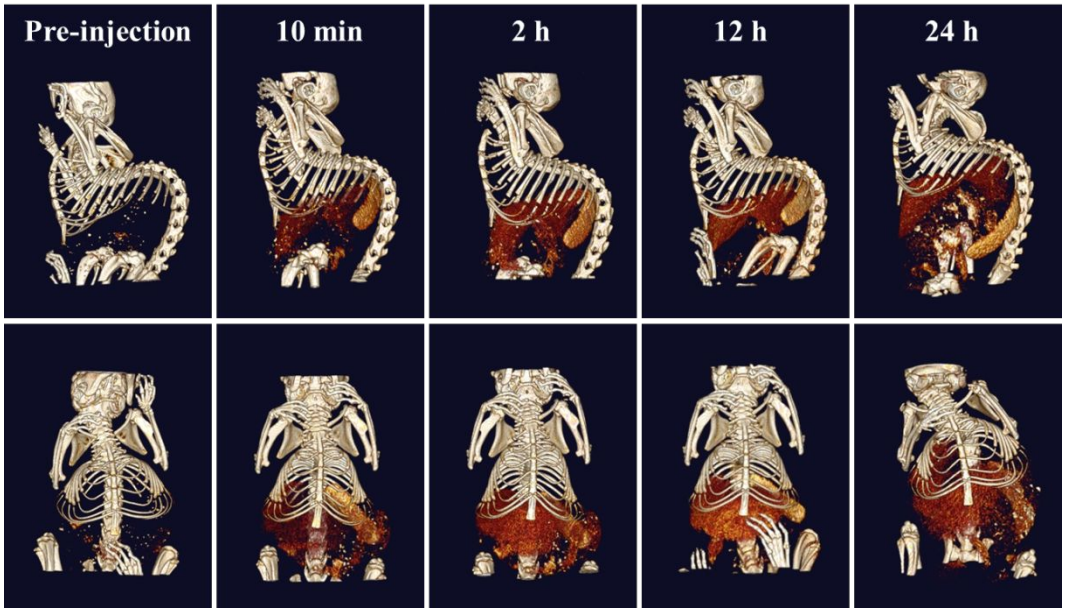

Figure S23. *In vivo* 3D volume-rendered CT imaging of Kunming mouse before and after intravenous injection of PAA-Lu-NRs (200 μL, 20 mg/mL) through tail vein at differenet time points.

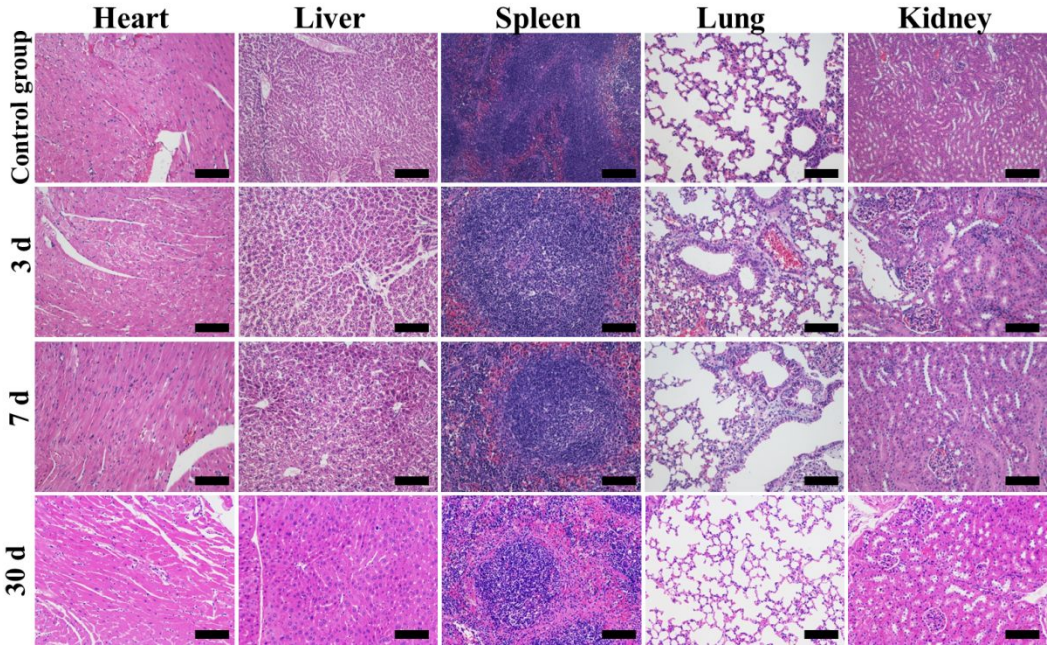

Figure S24. Histological changes of the mice injected with PAA-Lu-NRs for 3, 7 and 30 days and control group without injection. All the scale bars are 200 μm.

(s1) Li, Y. B.; Li, X. L.; Xue, Z. L.; Jiang, M. Y.; Zeng, S. J.; Hao, J. H. Second Near-Infrared Emissive Lanthanide Complex for Fast Renal-Clearable *In Vivo* Optical Bioimaging and Tiny Tumor Detection. *Biomaterials* **2018**, *169*, 35-44.

(s2) Xue, Z. L.; Zeng, S. J.; Hao. J. H. Non-Invasive Through-Skull Brain Vascular Imaging and Small Tumor Diagnosis Based on NIR-II Emissive Lanthanide Nanoprobes Beyond 1500 nm. *Biomaterials* **2018**, *171*, 153-163.

(s3) Zhong, Y. T.; Ma, Z. R.; Zhu, S. J.; Yue, J. Y.; Zhang, M. X.; Antaris, A. L.; Yuan, J.; Cui, R. Wan, H.; Zhou, Y.; Wang, W. Z.; Huang, N. F; . Luo, J.; Hu, Z. Y.; Dai, H. J. Boosting the Down-Shifting Luminescence of Rare-Earth Nanocrystals for Biological Imaging Beyond 1500 nm. *Nat. Commun*. **2017**, *8*, 737.

(s4) Antaris, A. L.; Chen, H.; Cheng, K.; Sun, Y.; Hong, G.; Qu, C.; Diao, S.; Deng, Z.; Hu, X.; Zhang, B.; Zhang, X.; Yaghi, O. K.; Alamparambil, Z. R.; Hong, X.; Cheng, Z.; Dai, H. A Small-Molecule Dye for NIR-II Imaging. *Nat. Mater*. **2016**, *15*, 235−242.

(s5) Li, W. J.; Nie, S. P.; Chen, Y.; Wang, Y. X.; Li, C.; Xie, M. Y. Enhancement of Cyclophosphamide-Induced Antitumor Effect by a Novel Polysaccharide from Ganoderma Atrum in Sarcoma 180-Bearing Mice. *J. Agric. Food Chem*. **2011**, *59*, 3707-3716.